Arabian Journal of Chemistry (2019) 12, 4848–4860

King Saud University

Arabian Journal of Chemistry

www.ksu.edu.sa
www.sciencedirect.com

ORIGINAL ARTICLE

# Photo-reduced route of polyaniline nanofiber synthesis with embedded silver nanoparticles

J. Bhadra [a], N.J. Al-Thani [a,*], S. Karmakar [b], N.K. Madi [a]

[a] Center for Advanced Materials, Qatar University, Qatar
[b] Department of Instrumentation and USIC, Gauhati University, India

Received 12 July 2016; accepted 2 October 2016
Available online 10 October 2016

KEYWORDS

Composite materials;
Electrical conductivity;
Nanostructures;
Activation energy;
Rietveld analysis

**Abstract** This work presents a method on the preparation and performance of four silver (Ag) concentrations in polyaniline (PANI) and polyvinyl alcohol (PVA) nanocomposite blend (PNPAg). The synthesis of Ag nanoparticles is first performed by photo reduction and then *aniline* is polymerized in Ag-PVA matrix. Morphological analysis by SEM and TEM reveals formation of nanoparticles with diameter 30–70 nm. Nanocomposites with lower Ag concentrations have highly aligned PNPAg nanofibers of diameter 50–80 nm and agglomeration for the one with higher concentrations. In addition, FTIR spectra show a systematic change in its characteristic peaks with increase in Ag contents. The crystallinity study depicts the tetragonal crystal structure of metallic nanocomposites having same particle sizes as obtained in SEM and TEM. In order to explore the possible applications of these nanocomposites in electronic industry, their electrical properties are investigated. The in-plane *I-V* characteristics indicate a transition of polymer nanocomposites from non-ohmic to ohmic material with increase of Ag content. The room temperature electrical conductivities are found to be in the range of $4.74 \times 10^{-4}$ to $3.96 \times 10^{-2}$ S/m with no major difference in activation energy for all nanocomposites.


## 1. Introduction

Cutting edge applications need a synergic combination of new hybrid material properties; therefore, it has attracted considerable attention over the years. A large number of research works have been carried out in this regard to obtain various potential nanomaterials with specific functionalities. Conducting polymer/metal nanocomposite is one such class of hybrid material. Enhanced optical, electrical and dielectric properties could well be obtained when polymer matrices are reinforced in different ratios with nanoscale fillers (Tamboli et al., 2012; Varga et al., 2012; Abbasi et al., 2015). Moreover, polymers play the key role in various potential applications in electronics industry (http://www.azom.com/article.aspx?ArticleID = 5969); electrically conducting polymers are also known as 'fourth-generation polymeric materials' (Heeger, 2001). Among the conducting polymers, polyaniline (PANI) has received significant research interest due to its distinct physical and chemical properties viz., redox properties, variable range of conductivity upon doping, ease of synthesis, and environmentally stable (http://www.azom.com/article.aspx?ArticleID = 1267). Due to these salient properties, PANI has obtained a wide variety of techno-

* Corresponding author. Fax: +974 4403 3989.
E-mail address: n.al-thani@qu.edu.qa (N.J. Al-Thani).
Peer review under responsibility of King Saud University.

Production and hosting by Elsevier

http://dx.doi.org/10.1016/j.arabjc.2016.10.001
1878-5352 

logical applications, for example, static charge dissipation, LED displays, electromagnetic shielding, gas sensors, pressure sensors, biosensors, transistors, and lightweight batteries to name a few (Li et al., 2009). Sometimes, commercial application of PANI gets limited due to its poor solubility, infusibility, processability and mechanical strength (Cardoso et al., 2007; Bhadra and Sarkar, 2009). To overcome these disadvantages, blending of PANI with other higher molecular weight polymers, for instance polyvinyl alcohol (PVA), is the most extensively studied method in recent years (Cardoso et al., 2007; Bhadra and Sarkar, 2009; Bhadra et al., 2014; http://www.4spepro.org/view.php?article=006131-2015-11-10). The good mechanical properties and intriguing electronic properties of these materials indicate that they can be used in various device applications.

At the same time, silver (Ag) and gold (Au) metal nanoparticles have gained considerable attention recently because of their promising technological applications and important properties (Sun and Xia, 2002; Zhang et al., 2013a). These properties have made Ag suitable for numerous applications such as catalysis, conductive inks, thick film pastes and adhesives for various electronic components, in photonics and in photography (Singh et al., 2011; Choudhury, 2009; Khanna et al., 2005; Fujii et al., 2011; Zhang et al., 2013b). Several approaches have already been employed to prepare conducting polymer–metal nanocomposite. Among them, blending of both components (Tamboli et al., 2012; Abbasi et al., 2015; http://www.azom.com/article.aspx?ArticleID=5969), polymerization of aniline monomer in the presence of metal nanoparticles (Wankhede et al., 2013), deposition of metal on conducting polymer using various oxidants (Stejskal et al., 2009; Blinova et al., 2009a), reduction of noble-metal compounds with PANI (Stejskal et al., 2009) and oxidation of aniline with noble-metal compounds (Blinova et al., 2009a, 2009b) are some of the simple ways. The photo-reduction process of metal is a novel and hassle-free method (because it does not need any harsh chemical resulting contamination free and environmental friendly method) for preparation of silver nanoparticles having desired shape and size with uniform distribution within the matrix (Choudhury, 2009; Pacioni et al., 2015).

Recently, one-dimensional (1D) PANI nanostructures (e.g., nanofibers and nanotubes) have attracted substantial attention because of their promising optoelectronic and chemo electronic properties. This is due to higher effective surface-to-volume ratio and shorter penetration depth for target molecules in comparison with their bulk counterparts. This leads them as a highly efficient material to be utilized in light-emitting diodes, electrical Nano devices, solar cells, and chemo sensors (Wanekaya et al., 2007; Chen et al., 2014; Huang et al., 2003). Most of the methods adopted for preparation of 1D polymer nanostructures are using hard or soft templates (Fujii et al., 2011; Zhang et al., 2013b). However, this technique produces unaligned 1D nanostructures and at the same time complete removal of the templates might be another challenge. As a result we have to compromise the purity of the samples. Despite having numerous attempts on successful fabrication of PANI nanofibers, there are limited numbers of reports for chemical synthesis of PANI aligned nanofibers.

In this paper, we propose a novel and hassle-free approach of synthesis for the aligned 1D PANI nanofibers by using photo-reduced Ag-PVA matrix as a reaction medium. We have presented a photoreduction method free from harsh chemicals to prepare Ag nanoparticles in PVA matrix followed by polymerization of aniline by in-situ polymerization in the same medium. Four different molar concentrations of $AgNO_3$ had been used to investigate their effect on the morphological and electrical properties of polymer nanocomposites in order to make it useful for electronic microchip application.

## 2. Materials & methods

This section describes the materials used and the methods adapted for characterizations of polymer blends.

### 2.1. Materials

All the chemicals and reagents used in this experiment are obtained from Merck (Germany) and Sigma chemical company and are of very high purity (99.9%). Aniline is purified by repeated distillation under vacuum and stored at low temperature prior to use. Polyvinyl alcohol used has a molecular weight (MW) of 30,000–50,000. The oxidizing agents such as ammonium persulfide and protonic acid are used without purification. All the solutions are prepared using double distilled water during synthesis.

### 2.2. Synthesis of Ag nanoparticles

Under constant stirring and heating (60 °C), 2 wt.% of PVA is dissolved in 200 ml of deionized (DI) water. We have studied the influence of two wavelengths, and they are as follows: UV-A (305 nm) and UV-B (390 nm). We have found that both the wavelengths have distinct effects on the size and shape of Ag nanoparticle. However, we have only completed the systematic analysis of UV-B and reported in this manuscript. In order to do the optimization of irradiation time, we have performed the experiment for 26 h of irradiation; the SEM images of silver nanoparticles have been taken at every hour. The images show that a specific particle size depends on the time until 24 h of irradiation; further increase in irradiation time does not have any significant effect on its particle size. Therefore, we have optimized our reduction time to 24 h. $AgNO_3$ is separately added to the PVA-DI gel as shown in Fig. 1. The operandi for the synthesis process of PVA-Ag nanocomposite using UV-visible light is given in Fig. 2; the reaction mechanism is similar to the procedure reported by Pandey et al. (2011). Four different concentrations, 0.5 M, 1.0 M, 1.5 M and 2.0 M, of $AgNO_3$-PVA-DI are prepared in PVA-DI solution. After exposing the above solutions with UV light for 24 h, finally, yellowish-red colloid of Ag nanoparticles uniformly dispersed in PVA is obtained. The scanning electron microscopy (SEM) and XRD both have confirmed that the average values of diameters for obtained Ag nanoparticles are ~30 nm and ~70 nm, respectively. At the same time, with the increase of Ag concentration the size of the nanoparticles is seen to have increased from 30 nm to 70 nm.

### 2.3. Synthesis of PNPAg nanocomposite and pure PANI

The PNPAg nanocomposite blend is synthesized by *in-situ* chemical polymerization of aniline monomer in the presence of Ag nanoparticles colloid dispersed in PVA matrix. In a typical synthesis process, aniline-DBSA (2.59 g, 20 mmol) is added to the already prepared Ag nanoparticles colloid (200 ml), followed by dropwise addition of the aqueous solution of Ammonium persulphate (5.71 g, 25 mmol). The aniline-DBSA composition is empirically obtained after a careful consideration from different combinations reported earlier by the authors (Bhadra et al., 2017). The resulting blend mixture is left to react for 24 h under constant stirring at 5–10 °C. The resultant product is made into thin film on glass slide and interdigitated gold electrode was washed with DI water and acetone. Thereafter, they are subject to drying in vacuum for 24 h. The preparation process of pure PANI is achieved by implementing same chemical polymerization technique as

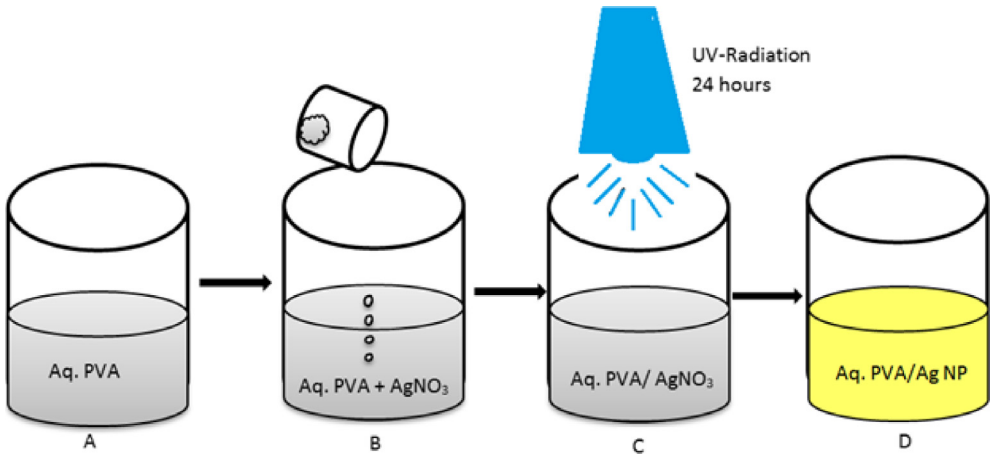


**Figure 1** Schematic representation of in situ reduction by UV radiation of $AgNO_3$ in aqueous PVA.

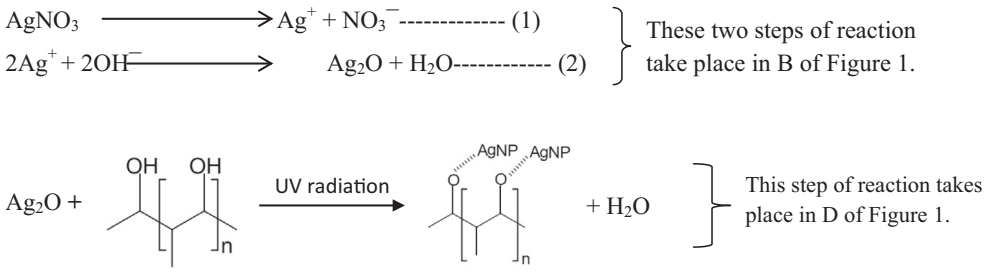


**Figure 2** Reaction mechanism of the synthesis of the PVA-Ag nanocomposites.

explained above but in the absence of Ag colloid. The methodology of nanofiber preparation is shown in Fig. 3.

### 2.4. Characterization techniques

#### 2.4.1. UV–Vis absorption spectroscopy

For UV–Vis spectroscopic analysis of ANI/Ag nanocomposite (colloidal solution) samples are dispersed and diluted respectably in ethanol. The absorption spectra are recorded on a Perkin Elmer Lambda 15 spectrophotometer.

#### 2.4.2. Morphological analysis

The morphologies of synthesized Ag-PVA and PANI/Ag nanocomposites are observed with a scanning electron microscopy (SEM) as well as transmission electron microscopy (TEM). Using a nano-SEM Nova 450 does SEM. The elemental compositions of PAPAg nanocomposites are estimated by energy dispersion X-ray (EDX).

#### 2.4.3. Fourier transform infrared (FTIR) spectroscopy

FTIR spectra of the nanocomposites are recorded on 8101 M, Shimadzu within the wavenumber range of 2000–400 $cm^{-1}$. The sample is prepared in the pellet form by mixing the material with KBr (Aldrich, 99%, FT-IR grade).

#### 2.4.4. UV-visible spectroscopy

UV-visible spectra are obtained by a Perkin Elmer Lambda 15 spectrophotometer for the wavelength range of 300–800 nm. The colloidal samples, before measuring, are diluted by using DI water.

#### 2.4.5. X-ray diffractometry (XRD)

X-ray diffraction patterns of PNPAg samples are recorded in a Philips (X'PERT PRO) Diffractometer using Cu Kα radiation ($\lambda$ = 1.5418 Å) at 40 kV and 30 mA with step size of 0.02 °C and with a speed of 1 s/deg. The diffractometer is calibrated with a standard silicon sample and the correction of broadening due slit width is also carried out.

#### 2.4.6. DC conductivity and temperature dependent conductivity

To measure the current-voltage (I-V) and electrical conductivity measurements, pure PANI (dispersing in m-cresol) and PNPAg nanocomposites are deposited on interdigitated finger electrode thick film Gold (15 mm × 15 mm) on alumina substrate-250 micron online/spaces alumina substrate. For temperature dependent measurements, pure PANI (dispersing in m-cresol) and PNPAg nanocomposites are coated on glass substrates. A homemade setup shown in Fig. 4 is used for this purpose.

## 3. Results and discussions

### 3.1. SEM results

The SEM results (given in Fig. 5(i)) reflect that there are changes in morphology of the PNPAg nano composites with

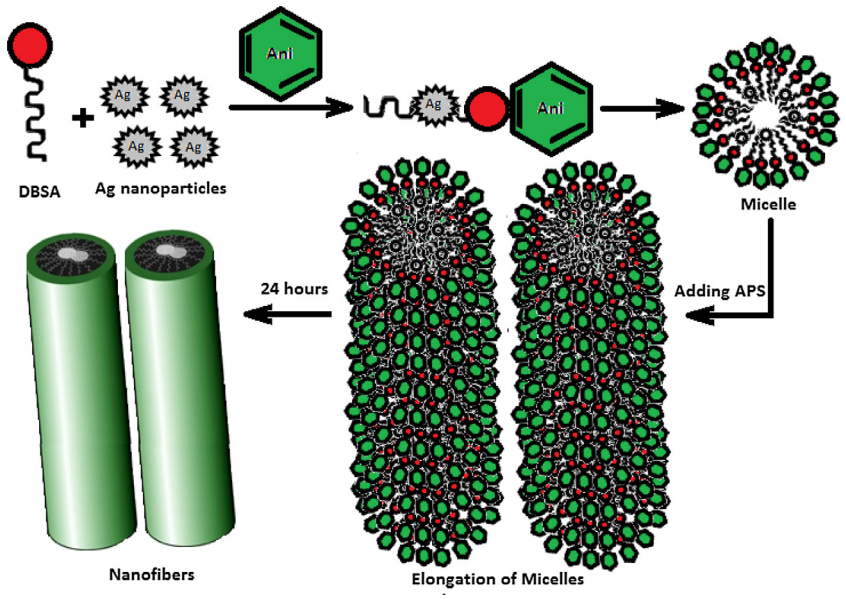


**Figure 3** Schematic on the synthesis of PAPAg nanofiber by chemical method.

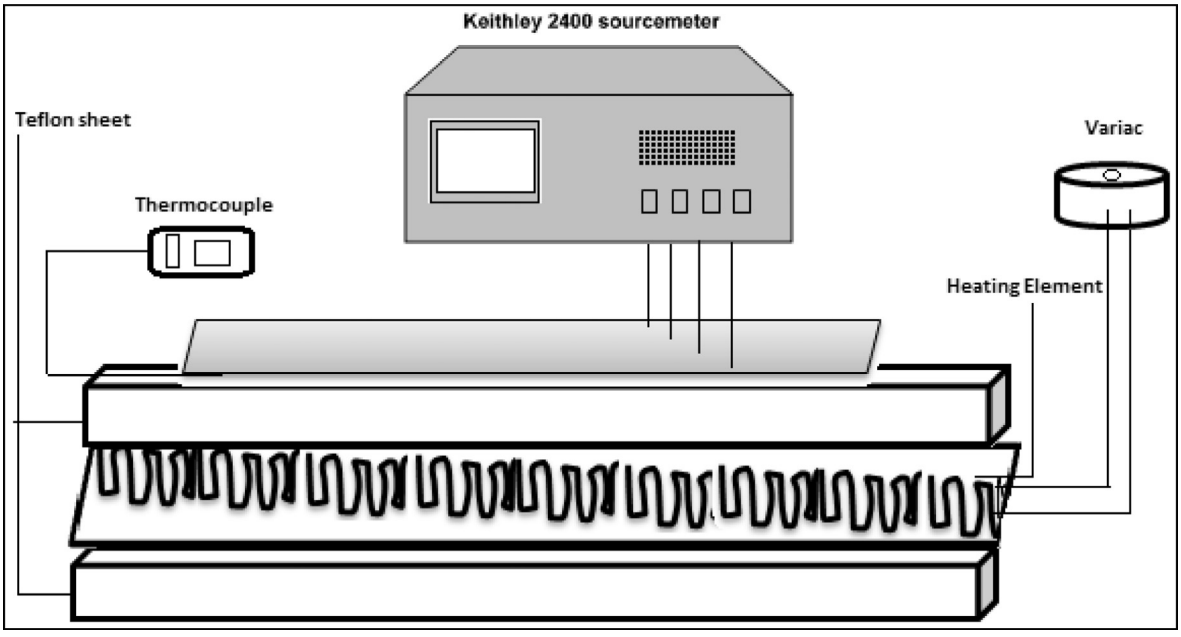


**Figure 4** Schematic diagram for temperature dependent conductivity measurement.

the change in Ag concentration. Inset in Fig. 5((ii), (iii)) shows the SEM of Ag nanoparticles dispersed in PVA matrix along with its EDX. The concentration of the Ag nanoparticles is observed to have increased with Ag concentration. For the PNPAg nanocomposites, first two lower concentrations of Ag, and the polymers with both low and high magnification show nanocomposite, structurally, to resemble nanowires with average diameter of about 50–80 nm with Ag particles embedded on it. A schematic diagram as shown in Fig. 4 demonstrates the mechanism behind the formation of nanofibers. The long tail surfactant (DBSA) assists in the formation of circular micelles, which further elongates to form aligned fibers. Table 1 provides the sizes of Ag nanoparticles and diameters of PNPAg nanofibers. However, for next higher concentrations of Ag, the fibers started to agglomerate and finally for the highest concentration, it forms some non-uniform particles. This could be due to inadequate quantity of surfactant (DBSA) to disperse all Ag nanoparticles and keep them separate (in case of 1.5 and 2.0 M of Ag); DBSA concentrations are kept constant while increasing Ag concentrations. EDX spec-

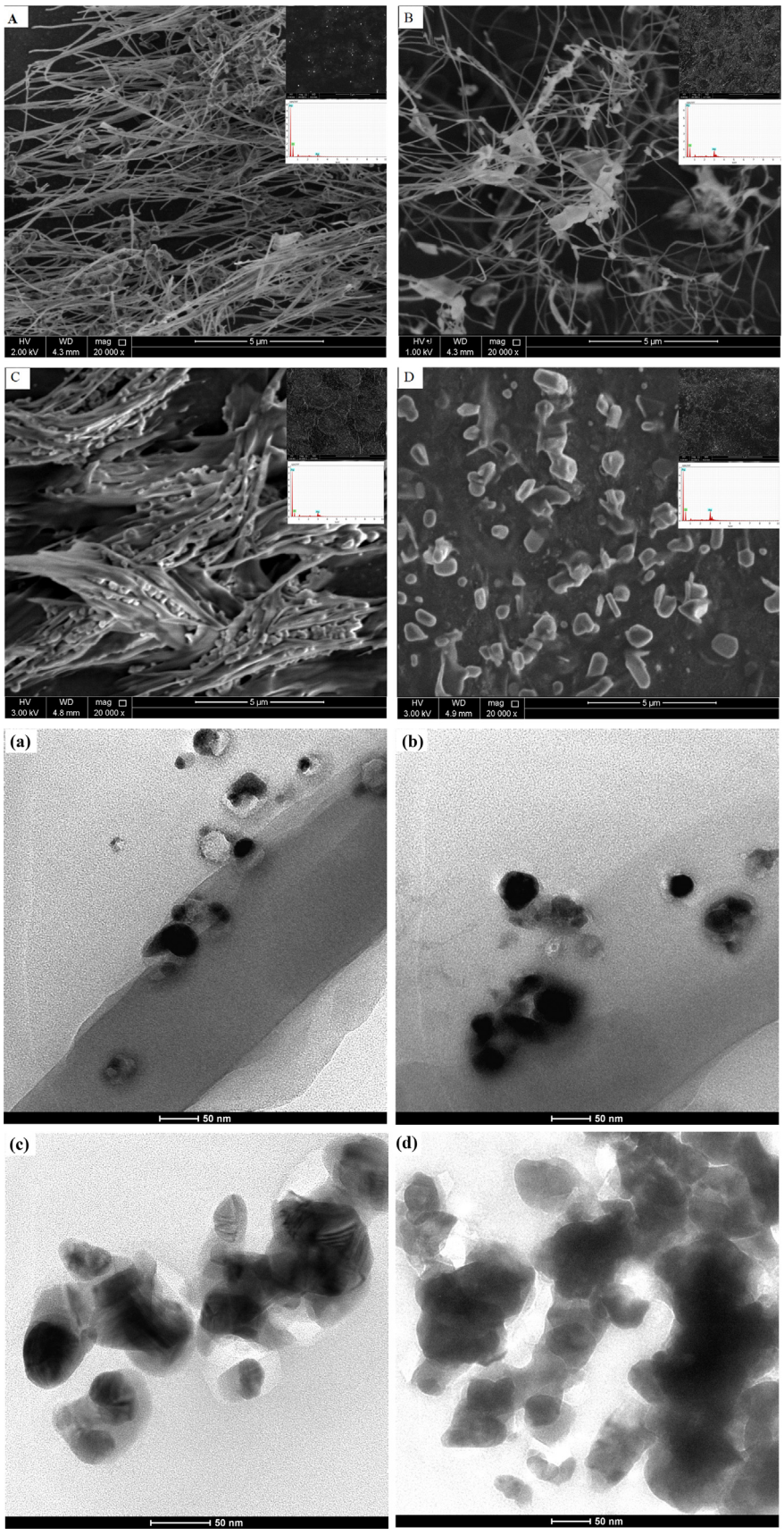


**Figure 5** (i) SEM picture for PNPAg nanocomposites (A) 0.5 M Ag, (B) 1.0 M Ag, (C) 1.5 M Ag, (D) 2.0 M Ag. (ii) Inset of the figures contain SEM of Ag nanoparticles dispersed in PVA matrix. (iii) Inset EDX of the Ag nanoparticles dispersed in PVA matrix. (iv) TEM images of nanocomposites: (a) 0.5 M Ag, (b) 1.0 M Ag, (c) 1.5 M Ag, (d) 2.0 M Ag.

**Table 1** Table containing crystal lattice parameters, particle size from both XRD, SEM and PNPAg nanofiber diameters.

| Sample. Code No. | Calculated lattice par (Å) | Corrected lattice par (Å) | Av. particle size by XRD nm | Particle size by SEM | Nanofiber diameter nm |
|---|---|---|---|---|---|
| Ag-0.5 | $a = b = 7.54(3)$<br>$c = 9.93(1)$ | $a = b = 7.53(3)$<br>$c = 9.94(2)$ | 42 | 35 | 50 |
| Ag-1.0 | $a = b = 9.70(1)$<br>$c = 7.54(4)$ | $a = b = 9.69(1)$<br>$c = 7.52(5)$ | 47 | 50 | 65 |
| Ag-1.5 | $a = b = 4.94(3)$<br>$c = 7.54(1)$ | $a = b = 4.93(2)$<br>$c = 7.53(1)$ | 64 | 60 | – |
| Ag-2.0 | $a = b = 9.87(2)$<br>$c = 12.34(2)$ | $a = b = 9.89(3)$<br>$c = 12.34(4)$ | 68 | 70 | – |

**Table 2** Table containing composition of Ag dispersed in PVA matrix.

| Samples ID | O % | Ag% |
|---|---|---|
| Ag-0.5 M | 98.99 | 1.01 |
| Ag-1.0 M | 95.28 | 4.72 |
| Ag-1.5 M | 94.05 | 5.95 |
| Ag-2.0 M | 93.51 | 6.49 |

tra are shown in inset of SEM; elemental composition (shown in Table 2) shows the presence of silver in the nanocomposite. The presence of O signals is believed to be due to PVA matrix.

Results of TEM analysis (Fig. 5(iv)) further agree with our conclusion that nanoparticles form in the range of 30–70 nm. For the first two lower contents of Ag, nanoparticles are seen to be well dispersed and embedded inside the nanofibers, whereas for remaining two, we see agglomeration of the metal particles as provided by SEM results.

### *3.2. FTIR characterization*

The FTIR analysis of pure and blend composite films is shown in Fig. 6. Two characteristic peaks at 1750 $cm^{-1}$ and 2375 $cm^{-1}$ are related to stretching vibration of carboxylic group (C═O) and (O—H) group, respectively; on the other hand, peaks at 2875 $cm^{-1}$ and 2940 $cm^{-1}$ are associated with the C—H group. These peaks are noticed in all the pure and blend spectra but with different intensities. The C—N stretch is a strong vibration when attached to the aromatic ring and in the nanocomposites, this mode has appeared as a small peak around 1250 $cm^{-1}$ (Jing and Xing, 2007; Neelgund et al., 2008). With the increase in the Ag concentration, there is a little shift as well as decrease in intensity of the peaks at 1250 $cm^{-1}$; this may be possible due to composite formation between PANI and silver (Jing and Xing, 2007). Relatively small peak at 1375 $cm^{-1}$ indicates the formation of S═O group. The peaks at 1562.5 $cm^{-1}$ and 1437 $cm^{-1}$ are assigned to C═N stretching of quinoid and C═C stretching of the benzoid rings, respectively (Cao et al., 2014). The characteristic bands at 1335 $cm^{-1}$ represent the C—N stretching of benzenoid structure. The bands at 1078 and 817 $cm^{-1}$ are identified as C—H in plane bending, 1,4-disubstituted benzene, and the out-of-plane bending of C—H bond in the aromatic ring. The band at 670 $cm^{-1}$ is detected due to Unsymmetric stretching vibration of S═O (DBSA).

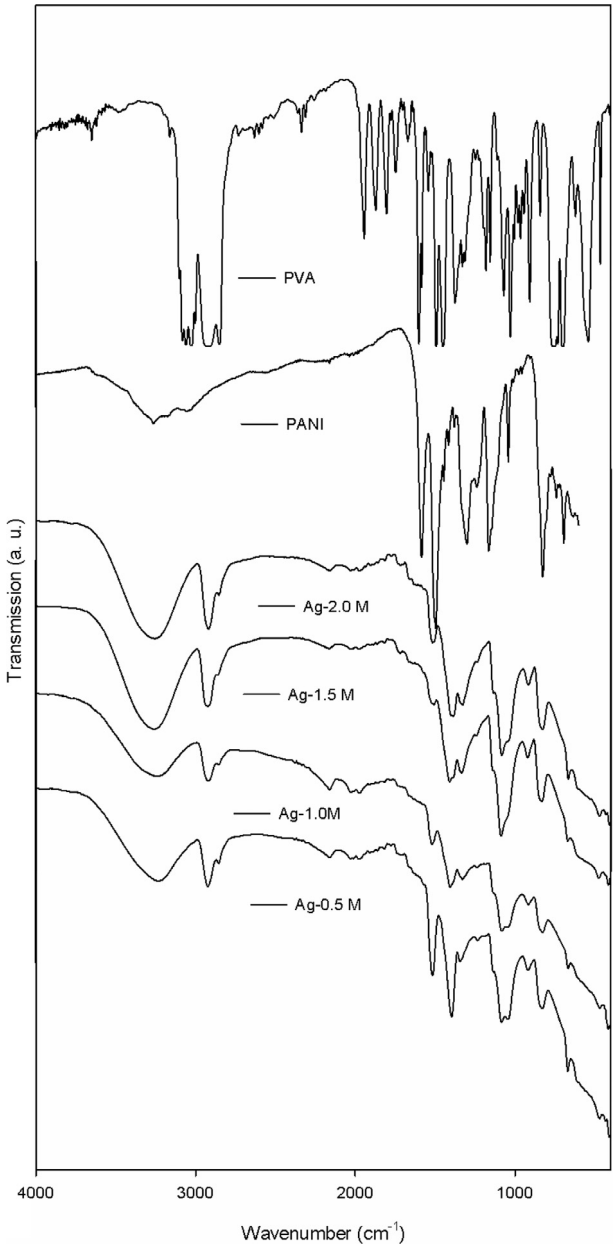


**Figure 6** FTIR of PNPAg nanocomposites and pure PANI and PVA.

### 3.3. UV–Vis

UV–Vis absorption spectra of PNPAg nanocomposites and inset show the spectra of Ag nanoparticles dispersed in PVA matrix are provided in Fig. 7. The characteristic absorption peak of Ag-PVA is noticed at 380–450 nm. This peak is attributed to surface plasmon resonance absorption of electrons in conducting silver (Zhang et al., 2002; Birla et al., 2013). Pure PVA only exhibits one absorption peak at 294 nm. For the composite samples there are two absorption peaks at 220–226 nm and at 396–420 nm, corresponding to the $\pi \rightarrow \pi^*$ of benzenoid rings and localized polarons (quinoid, Q), respectively. With the increase of Ag concentration it is found that the band at 396–420 nm gets broadened due to the increase in interaction between PANI and Ag. Another broad absorption peak is observed at 800 nm that is ascribed to an exciton located in the quinoid ring. Another phenomenon is observed when a conducting polymer–metal nanocomposite is excited by light photons that are coupled at the interface of polymer and metal. This results an induced charge density oscillation that gives rise to a strong absorption peak at a particular wavelength. With increase in Ag concentration in the blend this absorption peak shifts toward longer wavelengths, which could be due to the spill-out of the s-electrons or because of increase of the effective mass of the conduction electrons (de Heer, 1993).

### 3.4. XRD characterization

The X-ray diffraction patterns of PANI-Ag nanocomposite blends are shown in Fig. 8. The diffraction patterns show that the compound is polycrystalline in nature. It is seen that at concentration of 0.5 M (Ag-0.5) and 1.0 M (Ag-1.0), the degree of crystallinity of the PANI-Ag nanocomposites is almost same. But as the concentration is increased to 1.5 M (Ag-1.5) and 2.0 M (Ag-2.0), the degree of crystallinity is increased to a relatively very high value. The average particle sizes are found to be of the order of 42 nm (for Ag-0.5), 47 nm (for Ag-1.0), 64 nm (for Ag-1.5) and 68 nm (for Ag-2.0) with the increase in molarity. The particle sizes calculated by SEM are found to be of the order of 30–80 nm. The particle sizes measured by XRD and SEM are not exactly matched which is because of the fact that the XRD measures the average particle size in a direction perpendicular to some lattice planes and the SEM measures the particle size of an individual particle. The synthesized nanocomposites in all molarities are crystallized in Tetragonal system. The lattice parameters of the compounds are calculated using the standard Rietveld analysis method and are corrected by Nelson-Riley plot (McCusker et al., 1999; Culity, 1979). The lattice parameters and particle sizes of PANI-Ag of different molarities are shown in Table 1.

The corrected values of lattice parameters are estimated by Nelson-Relay plot which is a graph of calculated lattice parameters vs. error function. The equation of error function is as follows:

$$f(\theta) = \frac{1}{2}\left(\frac{\cos^2_\theta}{\sin\theta} + \frac{\cos^2_\theta}{\theta}\right) \quad (1)$$

where $\theta$ is the half of the Bragg angle.

Nelson-Riley plot for lattice constants of PANI-Ag with different molarities is shown in Fig. 9(A-H).

### 3.5. DSC characterization

Fig. 10 and Table 3 show the DSC thermogram of PANI nanocomposites indicating two exothermic peaks. The first broad peak starts at room temperature and ends at around

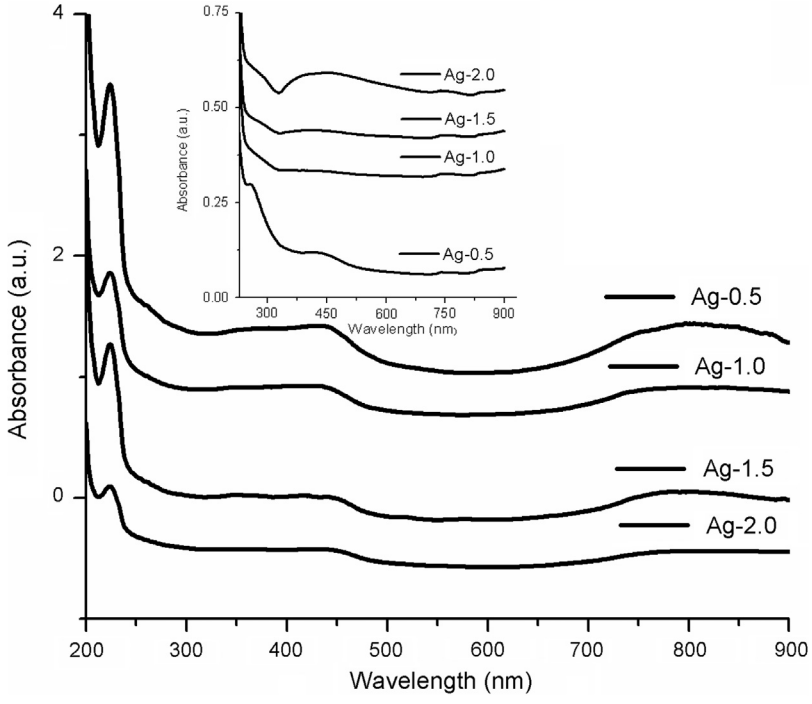


**Figure 7** UV–Vis of PNPAg nanocomposites and for pure PANI.

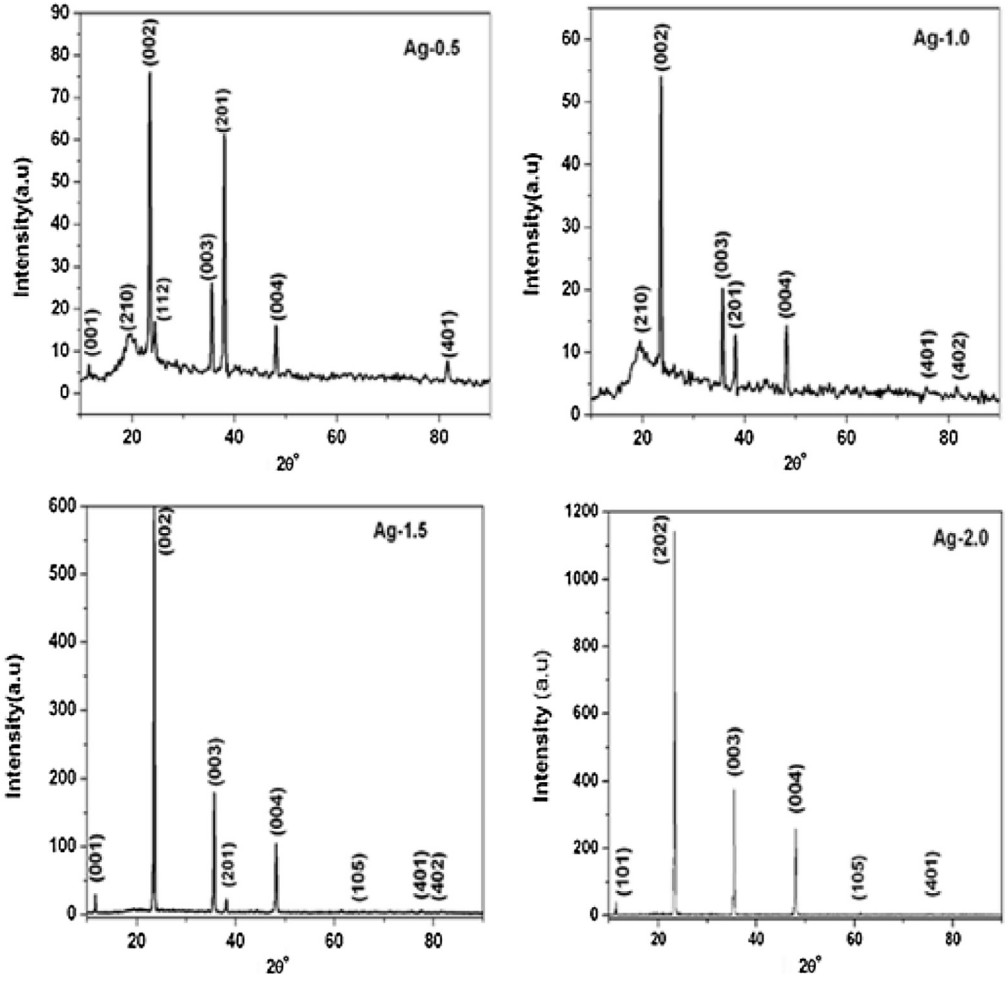


**Figure 8** X-ray diffraction pattern of PANI-Ag nanocomposites, Ag-0.5 (0.5 M), Ag-1.0 (1.0 M), Ag-1.5 (1.5 M) and Ag-2.0 (2.0 M).

170 °C. This peak is detected in all the nanocomposite blends, which corresponds to evaporation of water and all other solvents used during the synthesis process. The second sharp peak starts at around 180 °C and terminates at around 240 °C. This peak is seen to shift to lower temperature with increase of Ag concentration in the nanocomposite blend films. This peak corresponds to chemical interaction between polymers and nanoparticles and the results show that the bonding strength decreases with increase in Ag concentrations. Similar effect of metal concentrations on DSC peaks for polymer nanocomposites is also established in the literature (Rajakani and Vedhi, 2015).

### *3.6. TGA study*

The TGA thermogram of PNPAg nanocomposites is shown in Fig. 11 and Table 4. Five degradation peaks are detected in the nanocomposite samples, one in pure PVA, and three in pure PANI samples (Bhadra et al., 2013, 2014). The presence of silver content in the composite blends can conveniently be determined as a residue in TGA. The residue of TGA exactly corresponds to the different weight percentages of Ag used in the nanocomposite preparation (Mostafaei and Zolriasatein, 2012). At the same time, these thermograms also provide additional information about the composition of oxidation products and their degradation temperature. The first step of weight loss is seen below 100–120 °C, associated with sample humidity. The peak of weight loss in the first step is spotted increasing with increase in Ag content. The second step of weight loss, starting at 150.63 °C, is related with the sample deprotonation and loss of polymers and acids. The peak of degradation is noted at 200 °C for all the composites. The third step of degradation is observed to have started at 250 °C for all the composites. This degradation peak is found to decrease with the increase in Ag concentration. The fourth and fifth degradation peaks are observed between 430 and 500 °C. In both the cases, the degradation peaks are functions of Ag concentration. These two peaks are observed only in composite thermograms and are associated with the degradation of some chemical interaction between the polymers (PANI and PVA) (Bhadra et al., 2013; Palaniappan and Narayana, 1994).

### *3.7. I-V characterization*

The I-V characteristics for all the polyaniline-polyvinyl alcohol-silver nanocomposite films are measured from −5 to 5 volt and from 5 to −5 volt as shown in Fig. 12. It is observed that with increase in Ag concentration, the value of current

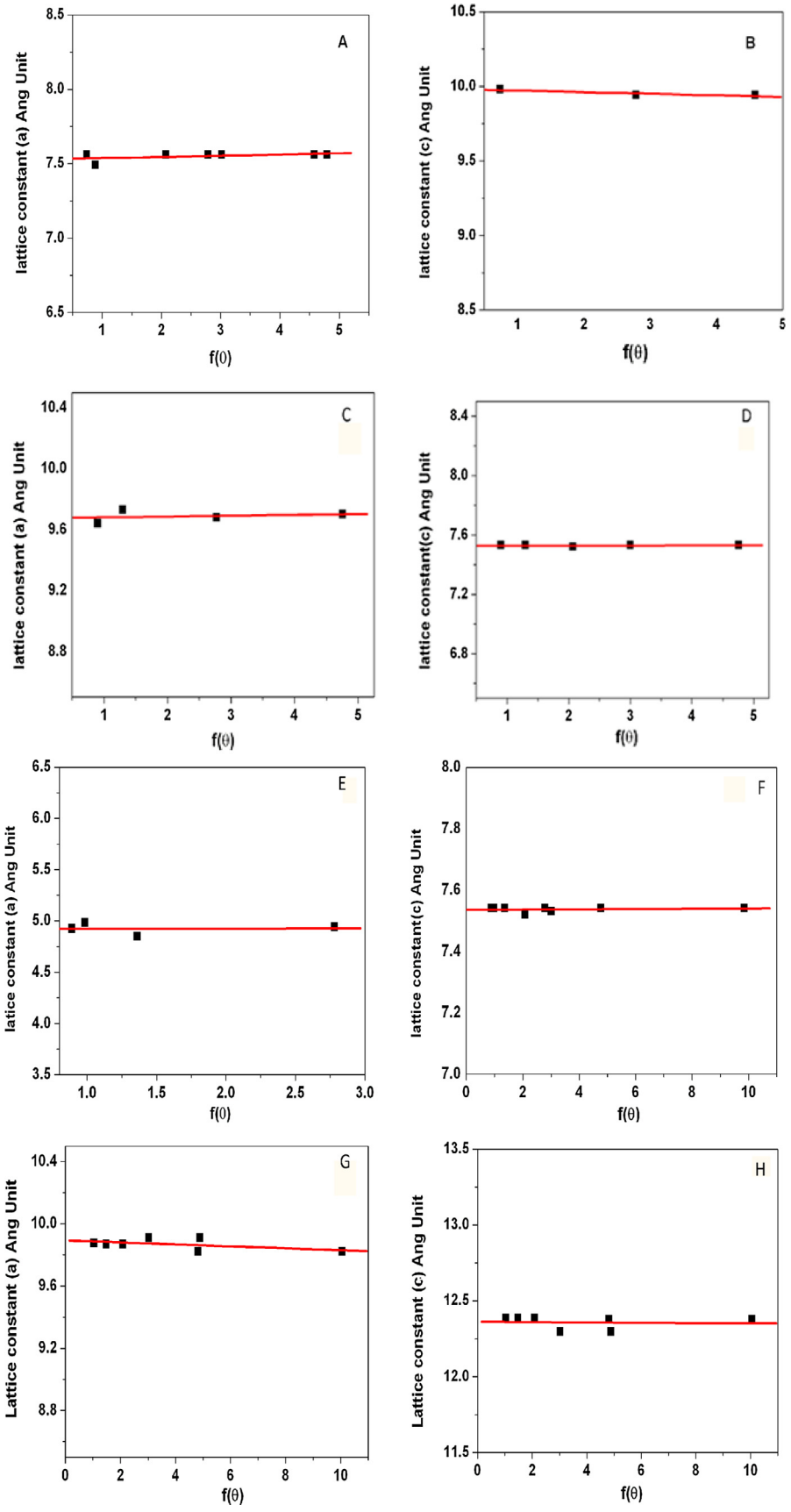


**Figure 9** Nelson Riley plot of Ag-0.5 for lattice constant '*a*' (A), for lattice constant '*c*' (B); of Ag-1.0 for lattice constant '*a*' (C), for lattice constant '*c*' (D); of Ag-1.5 for lattice constant '*a*' (E), for lattice constant '*c*' (F); of Ag-2.0 for lattice constant '*a*' (G) and for lattice constant '*c*' (H).

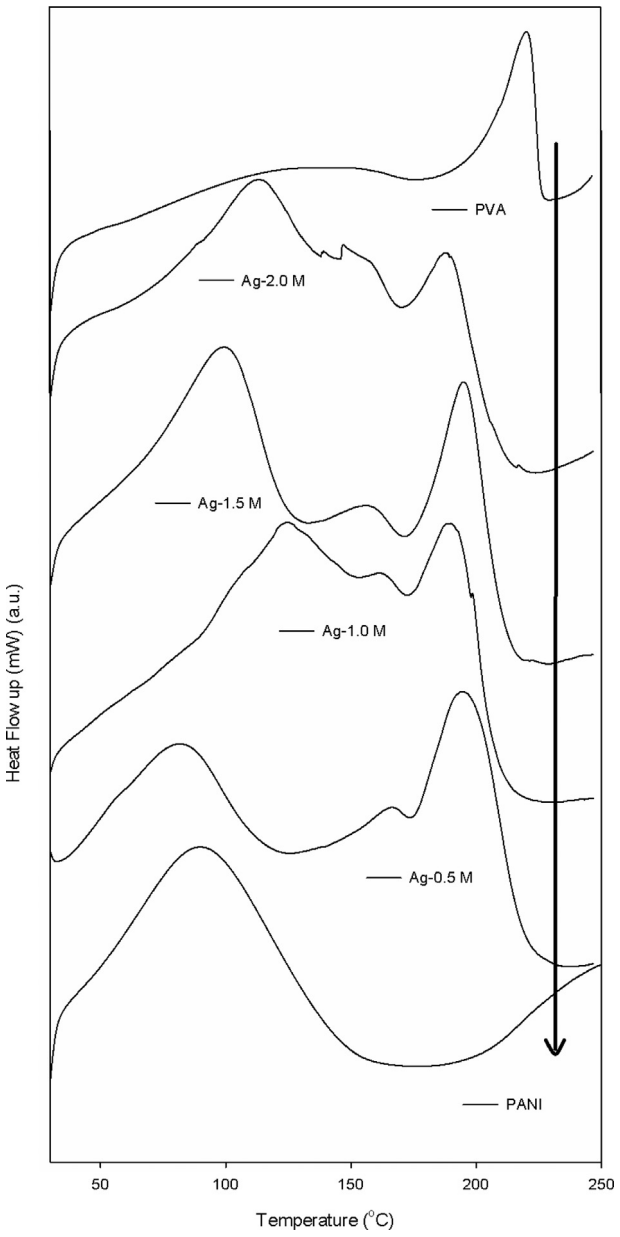


**Figure 10** DSC thermogram of PNPAg nanocomposites and for pure PANI and PVA.

**Table 3** DSC peak positions and $\Delta H$ values.

| Sample ID | Peak temperature (°C) | $\Delta H$ (J/g) |
|---|---|---|
| Ag-0.5 M | 220 | 64.84 |
| Ag-1.0 M | 218 | 58.39 |
| Ag-1.5 M | 215 | 50.37 |
| Ag-2.0 M | 214 | 46.38 |
| PANI | 259 | 174.03 |
| PVA | 220 | 59.94 |

corresponding to given voltage increases in the order of 10. The I-V characteristics for Ag 0.5 M and Ag 1.0 M are nonlinear as it corresponds to non-ohmic behavior. The results indicate that for lower concentration of Ag, the polymer

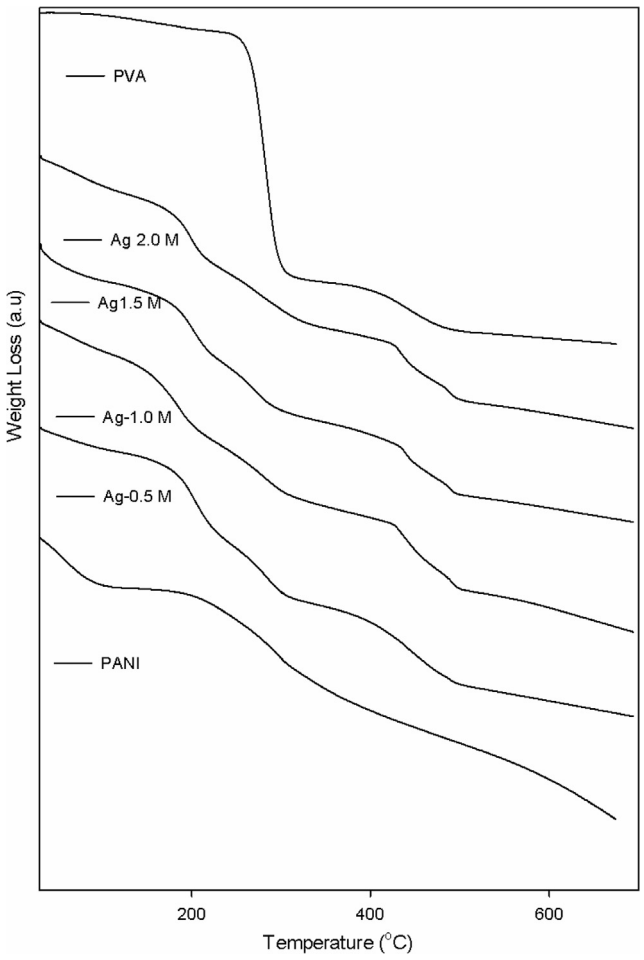


**Figure 11** TGA thermogram of PNPAg nanocomposites and for pure PANI and PVA.

nanocomposite has a semiconducting behavior. The I–V characteristic curve for Ag 0.5 M and Ag 1.0 M shows formation of hysteresis that indicates an electrical bistability representing a switching behavior. This phenomenon may be termed as the switching behavior having "on" and "off" states. However, with the increase of Ag concentration the non-ohmic nature gradually vanishes. It is found that for Ag 2.0 M, the obtained I-V characteristics is a straight line going through the origin indicating metallic behavior. Transition from non-ohmic to ohmic upon addition of metallic fillers is also observed in the literature (Oliveira et al., 2006; Somani et al., 1999). The mechanism behind this transition is explained in Section 3.8.

### *3.8. DC conductivity*

The room temperature dc conductivities of PANPAg nanocomposite synthesized with lowest and highest volume fraction of silver nanoparticles are 0.042 S/cm and 0.51 S/cm, respectively. Table 5 summarizes the values of composite and pure polymers. From the table, it is apparent that the dc electrical conductivities of the composites samples are higher than those of pure PANI and it increases with increase in Ag nanoparticle content in the composites. The increase in conductivity is justified due to electronic tunneling effect in the

**Table 4** Degradation peak positions for PNPAg nanocomposites and pure PANI and PVA and the weight percentage of residue left in PNPAg nanocomposites.

| Sample ID | TGA weight loss temperatures | | | | | |
|---|---|---|---|---|---|---|
| | 1st | 2nd | 3rd | 4th | 5th | Residue left |
| Ag-0.5 | 100 | 197 | 277 | 430 | 492 | 5% |
| Ag-1.0 | 110 | 196 | 272 | 432 | 488 | 10% |
| Ag-1.5 | 115 | 190 | 271 | 434 | 486 | 15% |
| Ag-2.0 | 120 | 190 | 270 | 434 | 485 | 20% |
| PANI | 100 | 203 | 291 | – | – | |
| PVA | – | – | 278 | – | – | |

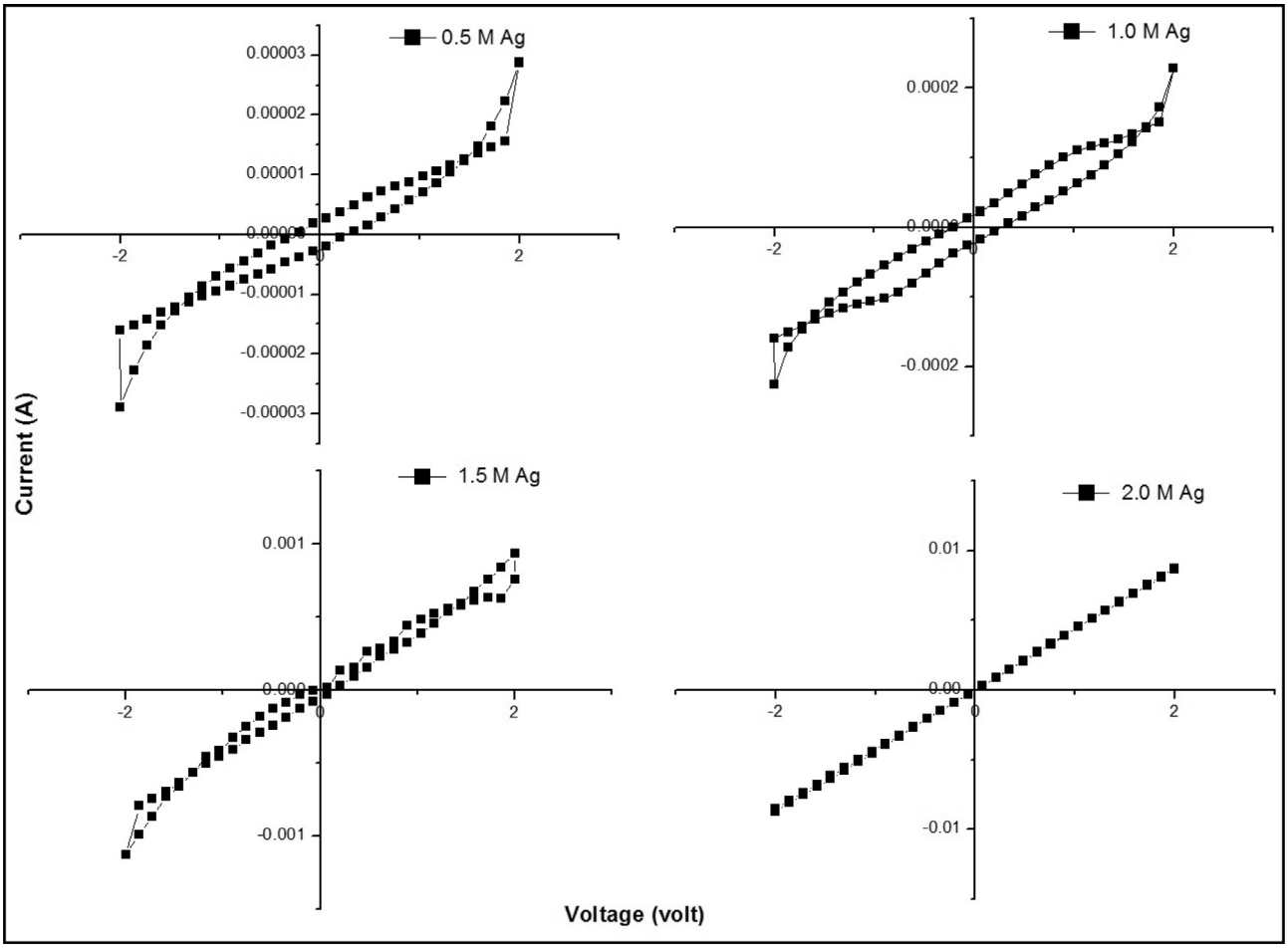


**Figure 12** I-V characteristics of PNPAg nanocomposites.

**Table 5** Room temperature conductivity and activation energy of the PNPAg nanocomposites and pure PANI and PVA.

| Sample ID | Conductivity (S/m) | Activation energy (eV) | |
|---|---|---|---|
| Ag-0.5 M | $4.73603 \times 10^{-4}$ | 0.0372375 | 0.146403 |
| Ag-1.0 M | $6.0804 \times 10^{-3}$ | 0.1244381 | 0.33844 |
| Ag-1.5 M | $7.32584 \times 10^{-3}$ | 0.22079339 | 0.326821 |
| Ag-2.0 M | $3.95594 \times 10^{-2}$ | 0.7148491 | 0.92684 |
| PVA | $1 \times 10^{-8}$ | – | – |
| PANI | $3.657 \times 10^{-3}$ | – | – |

polymer blend through Ag nanoparticles. For lower Ag nanoparticles loaded composite, the conductivity is marginal; however, as higher amount of nanoparticle is added, the increase in conductivity is significantly high that might be due to increase in the mobility of electron that leads to tunneling probability (Varga et al., 2012; Yılmaz et al., 2011; Gupta et al., 2010). Fig. 13 illustrates the formation process of conducting pathway with increase in Ag nanoparticles concentration. The schematic diagram depicts the procedure about how the increase in Ag concentration helps in decreasing the length of conducting path that leads to increase in conductivity (Wei

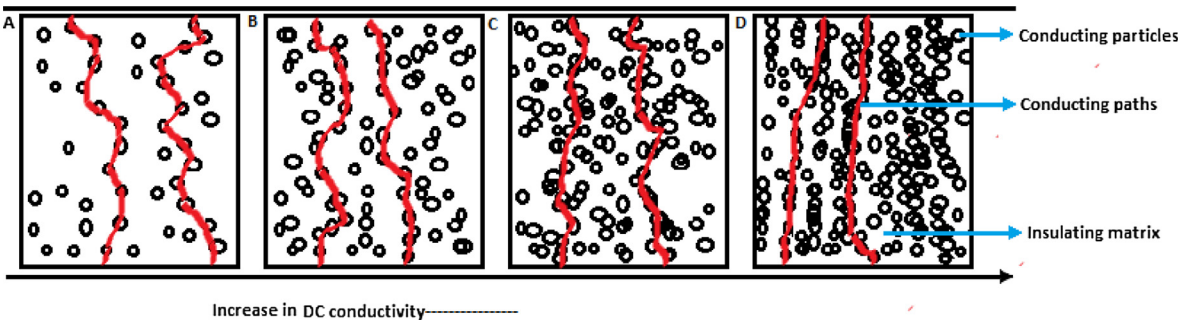


**Figure 13** Model on formation of conducting path: (A) 0.5 M Ag, (B) 1.0 M Ag, (C) 1.5 M Ag, (D) 2.0 M Ag.

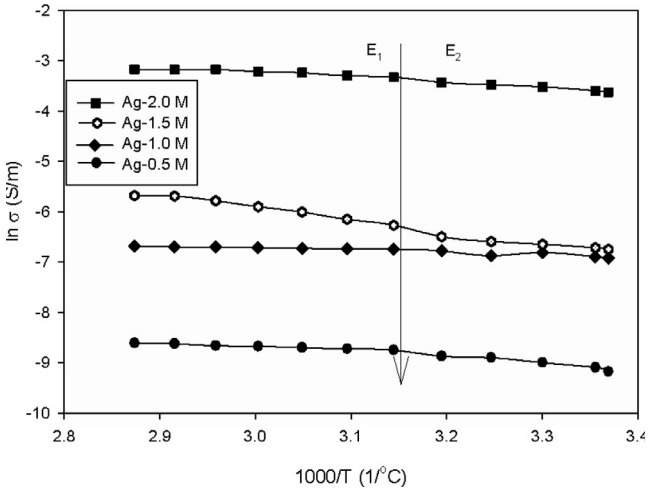


**Figure 14** Activation energy of the PNPAg nanocomposites.

and Eilers, 2009). As the concentration of the insulating matrix (PVA) is constant for all the composite films, its presence has no contribution to the conductivity.

Fig. 14 shows the variation of dc electrical conductivity with temperature in the range of 300–390 K for PANPAg nanocomposites. The behavior activation energy of composite films is studied by using Arrhenius equation:

$$\sigma_T = \sigma_o \exp(-E_a/k_B T) \tag{2}$$

where $\sigma_o$, $E_a$, $k_B$, and $T$ represent the pre-exponential factor, activation energy, Boltzmann constant ($8.617 \times 10^{-5}$ eV $K^{-1}$) and absolute temperature (K), respectively. The activation energy has been calculated by Eq. (2) from the slope of the straight line plot, ln $\sigma_T$ vs. $1/T$, shown in Fig. 14. Table 5 provides the values of activation energy calculated from the plot. From the values of activation energy it is evident that these values are nearly close to each other among the explored samples (Gupta et al., 2010; Tick and Fehlner, 1972). The value of activation energy generally depends on the radius of the metal particle present in the composition (Tick and Fehlner, 1972). The XRD and SEM analysis justifies that the average particle diameters are approximately 42, 47, 64 and 68 nm. This proves that the average particle diameters (of investigated samples) have nearly same order of magnitude. This is the reason why there is no major change in activation energy for all samples in this investigation (Wei and Eilers, 2009; Tick and Fehlner, 1972).

## 4. Conclusion

We have successfully synthesized Ag nanoparticles by UV-light photoreduction followed by chemical polymerization method for PNPAg nanocomposite preparation. The investigation confirms that PNPAg nanocomposite is more thermally stable and crystalline than pure PANI. The presence of Ag nanoparticles in the blend composite is evident from the data obtained by EDX, TEM, XRD, TGA and FTIR analysis. UV–Vis also shows the broadening of peak in optical absorption due to increase of Ag nanoparticle. Current voltage characteristic is noticed to transit from non-ohmic to ohmic as Ag content increases. Additionally, the room temperature electrical conductivity of the nanocomposite is found to have increased with Ag nanoparticles indicating that the conducting polymers can have enhanced structural, optical and electrical properties while forming nanocomposites. The lower Ag concentrations give rise to aligned nanofibers with particle dimension of 35–50 nm and formation of hysteresis can be observed as well. The I–V characteristic result indicates its possible potential application to develop electronic devices such as bistable switches and memory devices.

## Acknowledgment

The authors express their deep sense of gratitude to SAIF, Department of Instrumentation & USIC, Gauhati University, India, for XRD data collection.

## References

Abbasi, N.M., Yu, H., Wang, L., Abdin, Z., Amer, W.A., Akram, M., Khalid, H., Chen, Y., Saleem, M., Sun, R., Shan, J., 2015. Preparation of silver nanowires and their application in conducting polymer nanocomposites. Mater. Chem. Phys. 166, 1–15.

Bhadra, J., Sarkar, D., 2009. Self-assembled polyaniline nanorods synthesized by facile route of dispersion polymerization. Mater. Lett. 63, 69–71.

Bhadra, J., Al-Thani, N.J., Madi, N.K., Al-Maadeed, Mariam A., 2013. Preparation and characterization of chemically synthesized polyaniline–polystyrene blends as a carbon dioxide gas sensor. Synth. Met. 181, 27–36.

Bhadra, J., Madi, N.K., Al-Thani, N.J., Al-Maadeed, M.A., 2014. Polyaniline/polyvinyl alcohol blends: effect of sulfonic acid dopants on microstructural, optical, thermal and electrical properties. Synt. Met. 191, 126–134.

Bhadra, J., Al-Thani, N.J., Madi, N.K., Al-Maadeed, M.A., 2017. Effects of aniline concentrations on the electrical and mechanical properties of polyaniline polyvinyl, alcohol blends. Arab. J. Chem. 10(5), 664–672.

Birla, S.S., Gaikwad, S.C., Gade, A.K., Rai, M.K., 2013. Rapid synthesis of silver nanoparticles from fusarium oxysporum by

optimizing physicocultural conditions. Sci. World J. 2013, 796018. http://dx.doi.org/10.1155/2013/796018.
Blinova, N.V., Stejskal, J., Trchová, M., Sapurina, I., Ćirić-Marjanović, G., 2009a. The oxidation of aniline with silver nitrate to polyaniline–silver composites. Polymer 50, 50–56.
Blinova, N.V., Bober, P., Hromádková, J., Trchová, M., Stejskal, J., Prokeš, J., 2009b. Polyaniline/silver composites prepared by the oxidation of aniline with silver nitrate in acetic acid solutions. Polym. Int. 59, 437–446.
Cao, Y., Huang, R., Hu, B., Qiu, H., He, J., 2014. Structural and electrical properties of Ag films sputter-deposited on HCl-doped and undoped polyaniline substrates. Mater. Chem. Phys. 143, 788–793.
Cardoso, M.J.R., Lima, M.F.S., Lenz, D.M., 2007. Polyaniline synthesized with functionalized sulfonic acids for blends manufacture. Mater. Res. 10, 425–429.
Chen, X., Tang, Q., He, B., 2014. Efficient dye-sensitized solar cell from spiny polyaniline nanofiber counter electrode. Mater. Lett. 119, 28–31.
Choudhury, A., 2009. Polyaniline/silver nanocomposites: dielectric properties and ethanol vapour sensitivity. Sensors Actuat. B 138, 318–325.
Culity, B.D., 1979. Elements of X-ray Diffraction. Addison-Wesley Publishing Company, INC, pp. 327–335.
de Heer, W.A., 1993. The physics of simple metal clusters: experimental aspects and simple models. Rev. Mod. Phys. 65, 611–615.
Fujii, S., Kodama, M., Matsuzawa, S., Hamasaki, H., Ohtaka, A., Nakamura, Y., 2011. Conducting polymer-metal nanocomposite coating on fibers. In: Hashim, Abbass (Ed.), Advances in Nanocomposite Technology. ISBN: 978-953-307-347-7.
Gupta, K., Jana, P.C., Meikap, A.K., 2010. Optical and electrical transport properties of polyaniline–silver nanocomposite. Synth. Met. 160, 1566–1573.
Heeger, A.J., 2001. Semiconducting and metallic polymers: the fourth generation of polymeric materials. J. Phys. Chem. B 105, 8475–8491.
Huang, J., Virji, S., Weiller, B.H., Kaner, R.B., 2003. Polyaniline nanofibers: facile synthesis and chemical sensors. J. Am. Chem. Soc. 125, 314–315.
Jing, S., Xing, S., 2007. Lianxiang Yu, Yan Wu, Chun Zhao, synthesis and characterization of Ag/polyaniline core-shell nanocomposites based on silver nanoparticles colloid. Mater. Lett. 61, 2794–2797.
Khanna, P.K., Singh, N., Charan, S., Viswanath, A.K., 2005. Synthesis of Ag/polyaniline nanocomposite via an in situ photoredox mechanism. Mater. Chem. Phys. 92, 214–219.
Li, D., Huang, J., Kaner, R.B., 2009. Polyaniline nanofibers: a unique polymer nanostructure for versatile applications. Acc. Chem. Res. 42, 135–145.
McCusker, L.B., Von Dreele, R.B., Cox, D.E., Louer, D., Scardi, P., 1999. Overview of Rietveld refinement guidelines. J. Appl. Cryst. 32, 36–50.
Mostafaei, A., Zolriasatein, A., 2012. Synthesis and characterization of conducting polyaniline nanocomposites containing ZnO nanorods. Prog. Natl. Sci.: Mater. Int. 22, 273–280.
Neelgund, G.M., Hrehorova, E., Joyce, M., Bliznyuk, V., 2008. Synthesis and characterization of polyaniline derivative and silver nanoparticle composites. Polym. Int. 57, 1083–1089.
Oliveira, M.M., Castro, E.G., Canestraro, C.D., Zanchet, D., Ugarte, D., Roman, L.S., Zarbin, A.J.G., 2006. A simple two-phase route to silver nanoparticles/polyaniline structures. J. Phys. Chem. B 110, 17063–17069.
Pacioni, Natalia L., Borsarelli, Claudio D., Rey Valentina, Veglia Alicia V., 2015. Synthetic routes for the preparation of silver nanoparticles. In: Alarcon, E.I. et al. (Eds.), Silver Nanoparticle Applications, Engineering Materials. A Mechanistic Perspective © Springer International Publishing Switzerland; 2015. http://dx.doi.org/10.1007/978-3-319-11262-6_2.
Palaniappan, S., Narayana, B.H., 1994. Conducting polyaniline salts: thermogravimetric and differential thermal analysis. Thermochim. Acta 237, 91–97.
Pandey, S., Pandey, S.K., Parashar, V., Mehrotra, G.K., Pandeya, A. C., 2011. Ag/PVA nanocomposites: optical and thermal dimensions. J. Mater. Chem. 21, 17154.
Rajakani, P., Vedhi, C., 2015. Electrocatalytic properties of polyaniline–$TiO_2$ nanocomposites. Int. J. Ind. Chem. 6, 247–259.
Singh, R.P., Tiwari, A., Pandey, A.C., 2011. Silver/polyaniline nanocomposite for the electrocatalytic hydrazine oxidation. J. Inorg. Organomet. Polym. 21, 788–792.
Somani, P., Kale, B.B., Amalnerkar, D.P., 1999. Charge transport mechanism and the effect of poling on the current-voltage characteristics of conducting polyaniline-$BaTiO_3$ composites. Synth. Met. 106, 53–58.
Stejskal, J., Trchová, M., Kovářová, J., Brožová, L., Prokeš, J., 2009. The reduction of silver nitrate with various polyaniline salts to polyaniline–silver composites. React. Funct. Polym. 69, 86–90.
Sun, Y., Xia, Y., 2002. Large-scale synthesis of uniform silver nanowires through a soft, self-seeding, polyol process. Adv. Mater. 14, 833.
Tamboli, M.S., Kulkarni, M.V., Patil, R.H., Gade, W.N., Navale, S. C., Kale, B.B., 2012. Nanowires of silver–polyaniline nanocomposite synthesized via in situ polymerization and its novel functionality as an antibacterial agent. Colloids Surf. B 92, 35–41.
Tick, P.A., Fehlner, F.P., 1972. Electrical behavior of composite discontinuous films. J. Appl. Phys. 43, 362–368.
Varga, M., Prokeš, J., Bober, P., Stejskal, J., 2012. Electrical conductivity of polyaniline-silver nanocomposites, in: WDS'12 Proceedings of Contributed Papers, Part III, pp. 52–57.
Wanekaya, A.K., Bangar, M.A., Yun, M., Chen, W., Myung, N.V., Mulchandani, A., 2007. Field-effect transistors based on single nanowires of conducting polymers. J. Phys. Chem. C 111, 5218–5221.
Wankhede, Y.B., Kondawar, S.B., Thakare, S.R., More, P.S., 2013. Synthesis and characterization of silver nanoparticles embedded in polyaniline nanocomposite. Adv. Mat. Lett. 4, 89–93.
Wei, H., Eilers, H., 2009. From silver nanoparticles to thin films: evolution of microstructure and electrical conduction on glass substrates. J. Phys. Chem. Solids 70, 459–465.
Yılmaz, K., Akgoz, A., Cabuk, M., Karaagac, H., Karabulut, O., Yavuz, M., 2011. Electrical transport, optical and thermal properties of polyaniline–pumice composites. Mater. Chem. Phys. 130, 956–961.
Zhang, J.H., Li, X.L., Liu, K., Cui, Z.C., Zhang, G., Zhao, B., Yang, B., 2002. Thin films of Ag nanoparticles prepared from the reduction of AgI nanoparticles in self-assembled films. J. Colloid Interface Sci. 255, 115–118.
Zhang, J., Liu, X., Zhang, L., Cao, B., Wu, S., 2013a. Reactive template synthesis of polypyrrole nanotubes for fabricating metal/conducting polymer nanocomposites. Macromol. Rapid Commun. 34, 528–532.
Zhang, J., Liu, X., Wu, S., Xu, H., Cao, B., 2013b. One-pot fabrication of uniform polypyrrole/Au nanocomposites and investigation for gas sensing. Sensors Actuat. B 186, 695–700.